iScience

CellPress

Article

Viral Infection or IFN-α Alters Mitotic Spindle Orientation by Modulating Pericentrin Levels

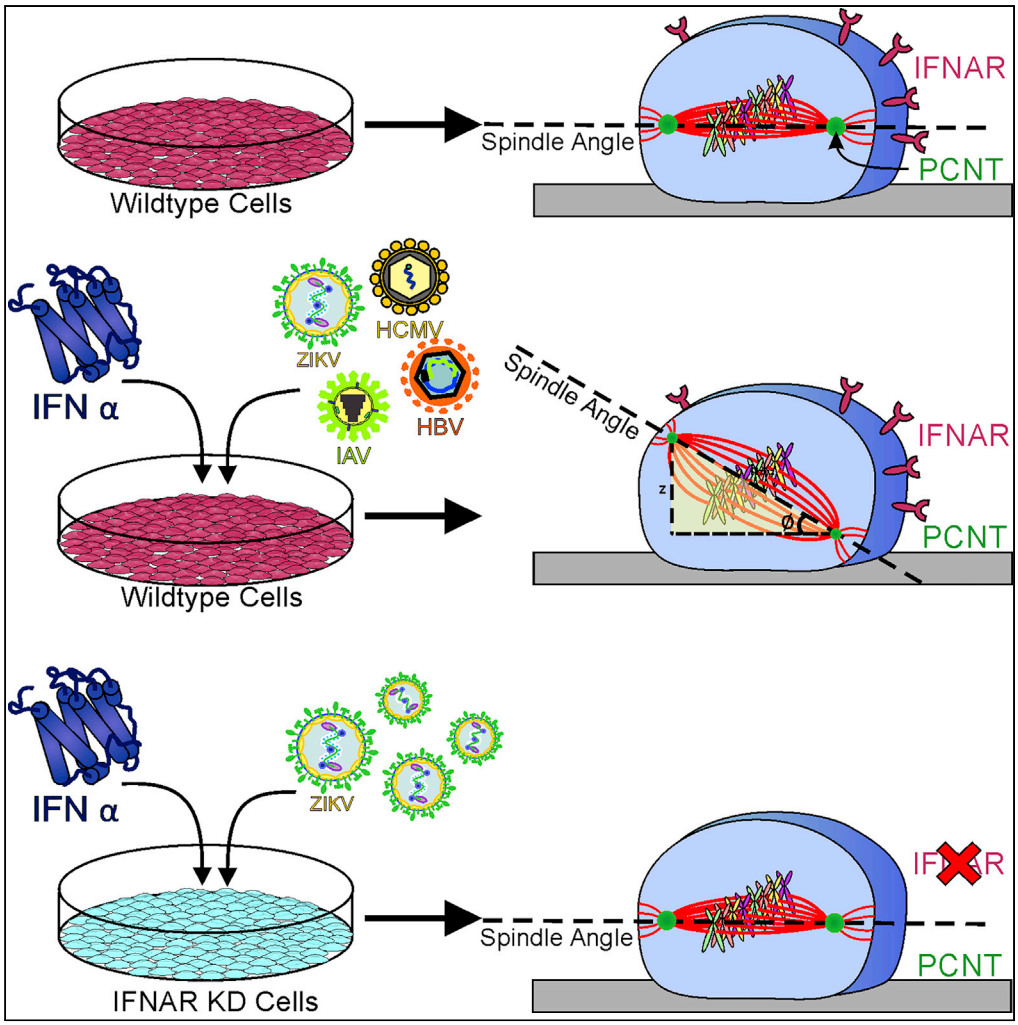

William M. McDougall, Jill M. Perreira, Hui-Fang Hung, ..., Timothy F. Kowalik, Stephen Doxsey, Abraham L. Brass

stephen.doxsey@umassmed.edu (S.D.)
abraham.brass@umassmed.edu (A.L.B.)

HIGHLIGHTS

ZIKV infection resembles MOPDII depletion of the centrosomal protein PCNT

Viral infection of mitotic cells results in loss of PCNT and spindle misorientation

IFN-α exposure to mitotic cells causes spindle misorientation

Loss of IFNAR abrogates both viral and IFN-α-induced spindle misorientation

McDougall et al., iScience *12*, 270–279
February 22, 2019
https://doi.org/10.1016/j.isci.2019.01.025

iScience

CellPress

Article

Viral Infection or IFN-α Alters Mitotic Spindle Orientation by Modulating Pericentrin Levels

William M. McDougall,[1] Jill M. Perreira,[1] Hui-Fang Hung,[2] Anastassiia Vertii,[3] E. Xiaofei,[1] Wendy Zimmerman,[4] Timothy F. Kowalik,[1] Stephen Doxsey,[4,*] and Abraham L. Brass[1,5,6,7,*]

SUMMARY

Congenital microcephaly occurs *in utero* during Zika virus (ZIKV) infection. The single-gene disorder, Majewski osteodysplastic primordial dwarfism type II (MOPDII), also leads to microcephaly and is concomitant with a decrease in the centrosomal protein, pericentrin (PCNT). This protein is a known contributor of mitotic spindle misorientation and ultimately, microcephaly. Similar to MOPDII, either viral infection or interferon (IFN)-α exposure reduced PCNT levels at the mitotic spindle poles. We unexpectedly found that infection of cells with any one of a diverse set of viruses, such as ZIKV, dengue virus, cytomegalovirus, influenza A virus, or hepatitis B virus, or treatment of cells with the anti-viral cytokine, IFN-α, produced mitotic spindle misorientation. These findings demonstrate a related mechanism for the development of microcephaly in viral infection, the host's antiviral IFN response, and primordial dwarfism.

INTRODUCTION

Zika virus (ZIKV) is a mosquito-borne flavivirus that has rapidly expanded its range across the world. Although ZIKV infection typically causes mild illness, it is associated with maternal infection and viral transmission to the fetus. The resultant congenital Zika syndrome can result in neurological insults, including microcephaly. Given ZIKV's impact on the health of newborns, it is important to understand how viral infection affects cellular physiology (Mlakar et al., 2016). Previous studies have shown that *in vitro* ZIKV infection alters cellular functions including mitosis, with infected cells demonstrating spindle misorientation and increased centrosome numbers (Gabriel et al., 2017; Onorati et al., 2016; Souza et al., 2016; Wolf et al., 2017). Infection of cells by a related flavivirus, dengue virus (DENV), produces comparable effects (Wolf et al., 2017).

Striking similarities between Majewski osteodysplastic primordial dwarfism type II (MOPDII) and congenital ZIKV syndrome include microcephaly. MOPDII is a rare autosomal recessive genetic condition presenting with dwarfism and microcephaly (Hall et al., 2004). In human patients, MOPDII is caused by mutations in the gene encoding the pericentrin (PCNT) protein (Rauch et al., 2008). Mice deficient in Pcnt ($Pcnt^{-/-}$) demonstrate many of the features of patients with MOPDII, including microcephaly (Chen et al., 2014).

During mitosis, PCNT recruits multiple proteins to the centrosome to generate the pericentriolar matrix (PCM) (Delaval and Doxsey, 2010). The PCM is required for the nucleation and organization of microtubules (Delaval and Doxsey, 2010). These processes are initiated by the phosphorylation of PCNT by Polo-like kinase 1 (PLK1) and are needed for centrosome maturation, which culminates in a fully assembled bipolar spindle (Doxsey et al., 1994; Haren et al., 2009; Lee and Rhee, 2011). The loss of PCNT compromises spindle pole integrity by preventing the essential congregation of microtubule-nucleating proteins (Chen et al., 2014). Bipolar spindle formation involves two distinct sets of microtubules, spindle microtubules, which bind to and carry chromosomes from the center of the spindle to the spindle poles during cytokinesis, and astral microtubules, which are anchored at the spindle poles and extend to the cellular cortex (Prosser and Pelletier, 2017). At the cortex, dynein motors bind to astral microtubules and generate forces that correctly orient the mitotic spindle (Prosser and Pelletier, 2017). Asymmetric division is the key mechanism in organ development that mediates both stem cell niche and cell differentiation. Asymmetric divisions rely on mitotic spindle orientation. Defects in proteins that are critical for proper spindle maintenance and orientation disrupt the balance between stem cell niche and differentiating progenitors. Thus spindle

[1]Department of Microbiology and Physiological Systems, University of Massachusetts Medical School, Worcester, MA 01605, USA

[2]Cell Biology Section, Neurogenetics Branch, National Institute of Neurological Disorders and Stroke, National Institutes of Health Bethesda, Bethesda, MD 20814, USA

[3]Department of Molecular, Cell and Cancer Biology, University of Massachusetts Medical School, Worcester, MA 01605, USA

[4]Program in Molecular Medicine University of Massachusetts Medical School, Worcester, MA 01605, USA

[5]Gastroenterology Division, Department of Medicine, University of Massachusetts Medical School, Worcester, MA 01605, USA

[6]Peak Gastroenterology Associates, Colorado Springs, CO 80907, USA

[7]Lead Contact

*Correspondence: stephen.doxsey@umassmed.edu (S.D.), abraham.brass@umassmed.edu (A.L.B.)

https://doi.org/10.1016/j.isci.2019.01.025

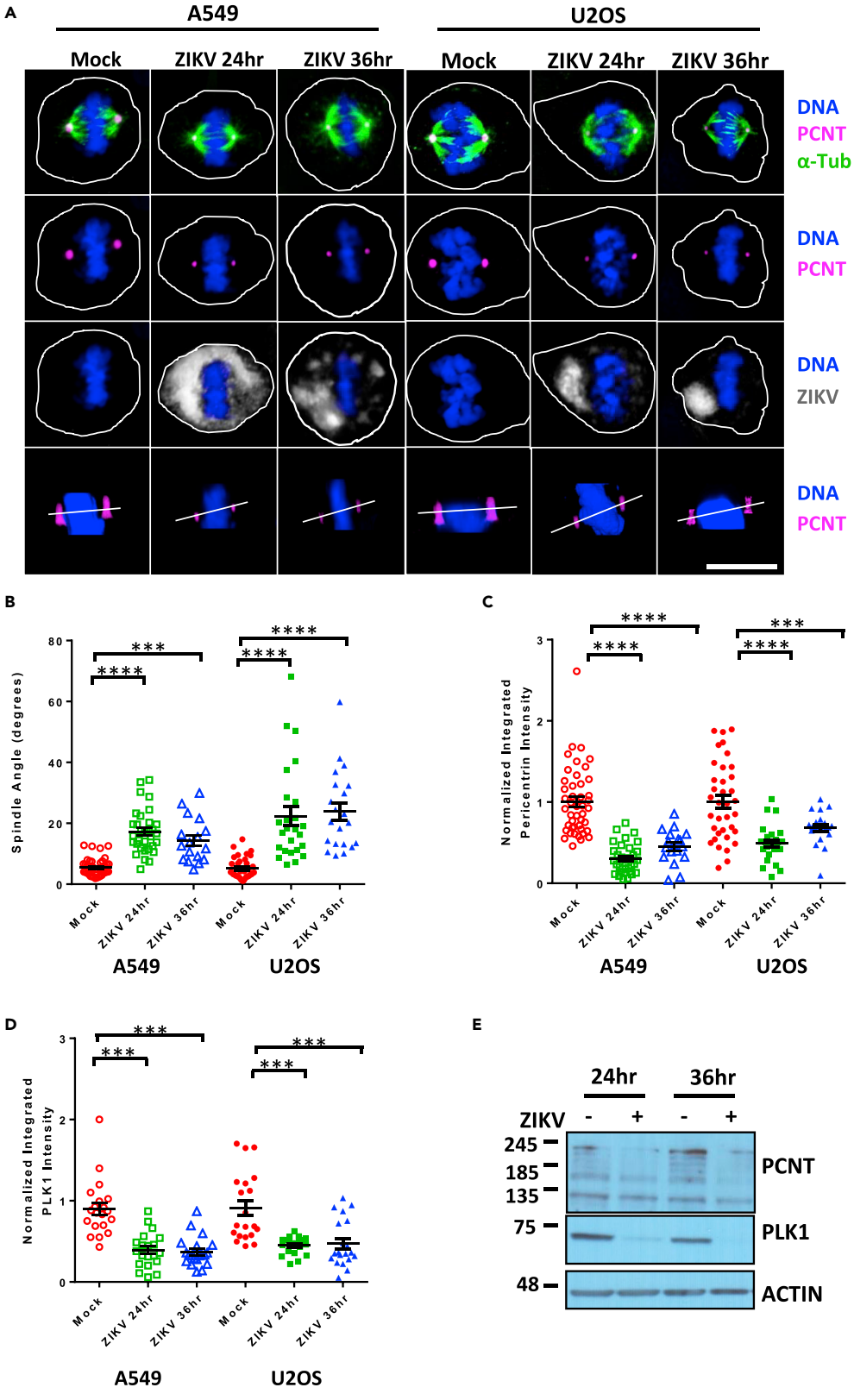
A
A549
U2OS
Mock
ZIKV 24hr
ZIKV 36hr
Mock
ZIKV 24hr
ZIKV 36hr
DNA
PCNT
α-Tub
DNA
PCNT
DNA
ZIKV
DNA
PCNT
B
Spindle Angle (degrees)
***
****
****
****
Mock
ZIKV 24hr
ZIKV 36hr
Mock
ZIKV 24hr
ZIKV 36hr
A549
U2OS
C
Normalized Integrated Pericentrin Intensity
****
****
***
****
Mock
ZIKV 24hr
ZIKV 36hr
Mock
ZIKV 24hr
ZIKV 36hr
A549
U2OS
D
Normalized Integrated PLK1 Intensity
***
***
***
***
Mock
ZIKV 24hr
ZIKV 36hr
Mock
ZIKV 24hr
ZIKV 36hr
A549
U2OS
E
24hr
36hr
ZIKV
-
+
-
+
245
185
135
75
48
PCNT
PLK1
ACTIN

Figure 1. ZIKV Infection Produces Spindle Misorientation and Decreases PCNT and PLK1 at the Spindle Poles

(A) Confocal images of A549 (left), or U2OS(right) cells in metaphase (xz plane), either mock infected (mock) or infected with ZIKV (PRVABC59 MOI 5) for 24 or 36 hpi and immunostained for PCNT (pink), α-Tub (green), and ZIKV (gray) and stained for DNA (blue). The bottom row of images shows an xz plane with a white line connecting the two spindle poles to approximate the spindle pole angle. Scale bars for all images, 10 μm.

(B) Spindle pole angle quantification for ZIKV infections of A549 or U2OS cells for mock infected (red, 46 A549 cells quantitated), 24 hpi (green, 32 cells), and 36 hpi (blue, 17 cells).

(C) Quantification of normalized PCNT intensity at the spindle poles for ZIKV infections of A549 or U2OS cells analyzed in (B), for mock infected (red), 24 (green), and 36 hpi (blue).

(D) Quantification of normalized PLK1 intensity at the spindle poles for ZIKV infections of A549 or U2OS cells analyzed in (B), for mock infected (red), 24 hpi (green), and 36 hpi (blue).

(E) Immunoblot of the indicated proteins from A549 cell lysates that were mock infected (−) or infected (+) with ZIKV at 24 and 36 hpi. Actin serves as a loading control. Molecular weights in kilodaltons are provided on the left. Statistical significance (p value) of the angle changed or integrated intensity between mock and a condition in all quantified data is represented using asterisks above the data; ****$p < 0.0001$, ***$p < 0.001$. All data represent the mean ± SEM from three independent experiments.

orientation defects (misoriented divisions) result in premature differentiation of neural progenitors (Vertii et al., 2018). Spindle misorientation occurs in the dividing cells of patients with MOPDII and the cells of $Pcnt^{-/-}$ mice (Chen et al., 2014). In both instances, the loss of PCNT prevents the proper growth and organization of the astral microtubules, leading to misoriented cell divisions and thus to skeletal and neurological defects, including microcephaly (Chen et al., 2014; Delaval and Doxsey, 2008; Hung et al., 2016; Rauch et al., 2008).

In this study we first examined the effect of ZIKV infection on cell division *in vitro*. In keeping with a previous report, we detected spindle misorientation in both ZIKV- and DENV-infected cells. We then expanded upon these observations by demonstrating that ZIKV infection of cells results in a decrease in the levels of PCNT similar to those observed in the cells from patients with MOPDII or from $Pcnt^{-/-}$ mice. We demonstrate that viral infection leads to decreased levels of PLK1, a kinase that is essential for PCNT phosphorylation and centrosome maturation. Moreover, we report that spindle misorientation occurs in cells infected with any of the following viruses: cytomegalovirus (CMV; herpesvirus), influenza A virus (IAV; orthomyxovirus), and hepatitis B virus (HBV; hepadnavirus). We found that treatment of cells with interferon (IFN)-α produced spindle misorientation, suggesting that the observed aberrations in mitosis may arise from viral infection triggering an IFN response. These findings have implications for maternal-fetal health and suggest that a shared mechanism underlies the development of microcephaly in viral infection, the host's antiviral IFN response, and primordial dwarfism.

RESULTS

Infection with ZIKV Produces Spindle Misorientation and Decreases PCNT and PLK1

ZIKV infection *in utero* is associated with birth defects, including microcephaly (Mlakar et al., 2016). Microcephaly is present in patients with MOPDII, and dividing cells from these patients demonstrate spindle misorientation (Chen et al., 2014). Therefore we investigated if the effect of ZIKV infection *in vitro* is similar to what has been reported in cells from patients with MOPDII. Lung adenocarcinoma (A549) and osteosarcoma (U2OS) cells were infected with ZIKV (Puerto Rico, December 2015, PRVABC59, MOI 5) for either 24 or 36 h. Confocal images of infected mitotic A549 cells showed that spindle misorientation occurred at both 24 and 36 h post infection (hpi), when compared with uninfected controls (mock, Figures 1A and 1B). In uninfected A549 cells, spindle angles were 4–5°. In ZIKV-infected cells the spindle angle increased to 19.5° (24 hpi) and 17.5° (48 hpi) (Figure 1B). Comparable increases in spindle angles with infection were seen with U2OS cells (Figure 1B). MOPDII cells undergoing mitosis have spindle pole misorientation and decreased levels of PCNT at the spindle poles (Chen et al., 2014). Therefore we evaluated ZIKV-infected mitotic A549 cells using confocal imaging; these studies revealed that PCNT intensity at the spindle poles of infected mitotic cells was lower than that in uninfected control mitotic cells at both 24 and 36 hpi (Figure 1C). Mitotic U2OS cells infected with ZIKV also exhibited lower levels of PCNT at their spindle poles when compared with uninfected control mitotic cells (Figure 1C). We further examined a key mitotic kinase, PLK1, which is required for recruiting multiple PCM components (including PCNT) to spindle poles during G2/M phase (Haren et al., 2009). PLK1 intensity at the spindle poles was also lower in both A549 and U20S mitotic cells infected with ZIKV at 24 and 36 hpi (Figure 1D).

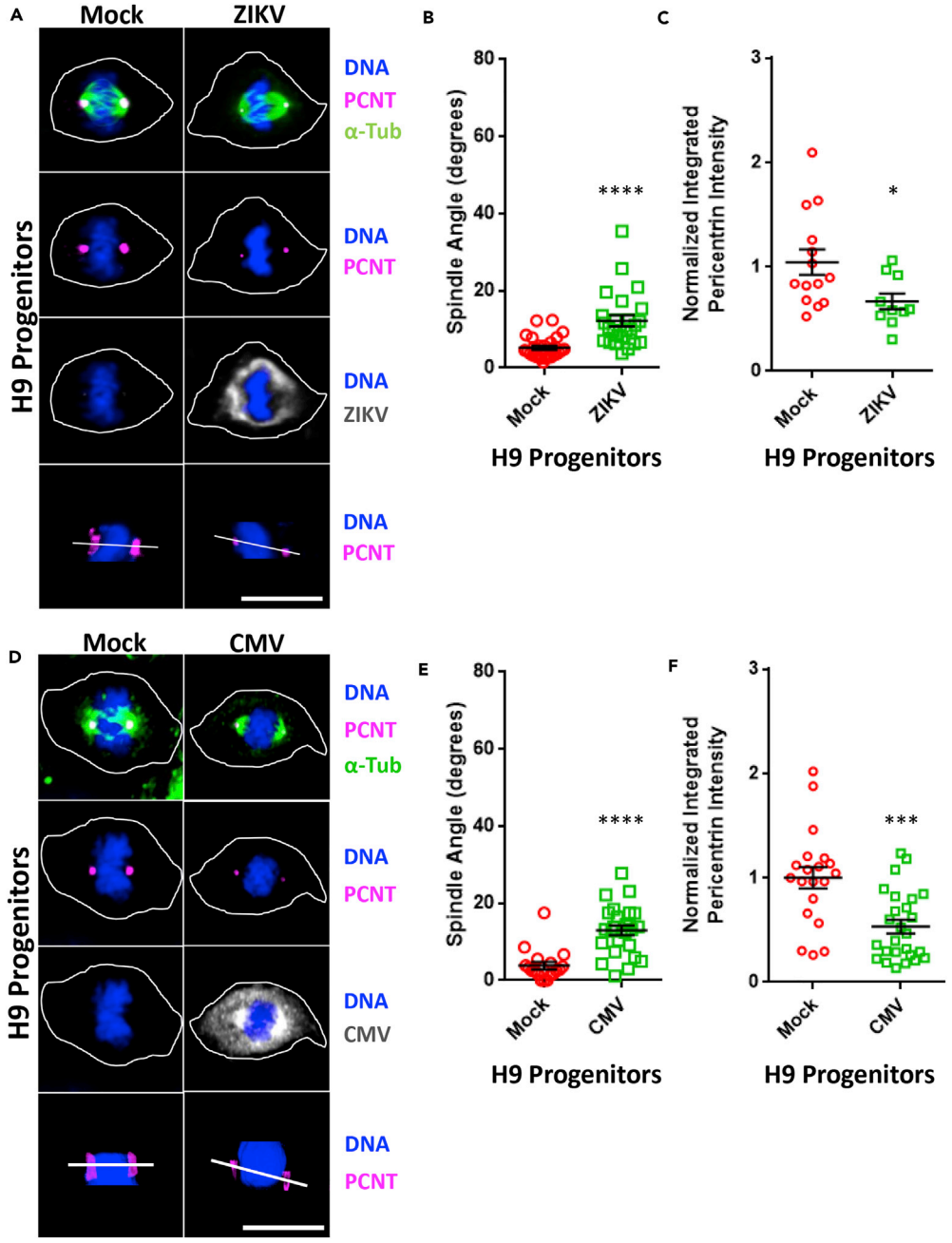

Figure 2. Infection of Neural Progenitor Cells with ZIKV or CMV Produces Spindle Misorientation and Decreases PCNT at the Spindle Poles

(A) Confocal images of H9 human neural progenitor cells in metaphase (xz plane), which have been either mock infected (mock) or infected with ZIKV (PRVABC59 MOI 5) for 24 h and immunostained for PCNT (pink), α-Tub (green), or ZIKV (gray) and stained for DNA (blue). The bottom row of images shows an xz plane with a white line connecting the two spindle poles to approximate the spindle pole angle. Scale bars for all images, 10 μm.

(B) Spindle pole angle quantification for ZIKV infections of H9 cells for mock infected (red, 29 cells quantitated) and 24 hpi (green, 25 cells).

(C) Quantification of normalized PCNT intensity at the spindle poles for ZIKV infections of H9 cells analyzed in (B), for mock infected (red) and 24 hpi (green).

(D) Confocal images of H9 human neural progenitor cells in metaphase (xz plane), which have been either mock infected (mock) or infected with CMV (TB40E-GFP MOI 3) for 24 hpi and immunostained for PCNT (pink), α-Tub (green), or CMV

Figure 2. *Continued*

(gray) and stained for DNA (blue). The bottom row of images shows an xz plane with a white line connecting the two spindle poles to approximate the spindle pole angle. Scale bars for all images, 10 μm.

(E) Spindle pole angle quantification for CMV infections of H9 cells for mock infected (red, 18 cells quantitated) and 24 hpi (green, 25 cells).

(F) Quantification of normalized PCNT intensity at the spindle poles for CMV infections of H9 cells analyzed in (E), for mock infected (red) and 24 hpi (green). Statistical significance (p value) of the angle changed or integrated intensity between mock and a condition in all quantified data is represented using asterisks above the data; ****$p < 0.0001$, ***$p < 0.001$, *$p < 0.5$. All data represent the mean ± SEM from three independent experiments.

We evaluated the effects of ZIKV infection on the cellular levels of PCNT and PLK1 using immunoblotting of whole-cell lysates from uninfected or infected cells. These studies showed that PCNT and PLK1 were both decreased after viral infection (Figure 1E). One explanation for these observations could be that the decrease in PCNT and PLK1 was due to loss of cell-cycle progression during infection. To evaluate this notion, A549 cells were serum starved for 48 h to synchronize them in G0 and then infected with ZIKV for 48 h. After infection, propidium iodide staining indicated that ZIKV infection had no effect on cell-cycle progression under these conditions (Figure S1A). A modest increase in γ-tubulin intensity was observed in ZIKV-infected mitotic cells (Figure S1B), along with the accumulation of NuMA at spindle poles (Figure S1C). Together these data revealed that infection with ZIKV results in events similar to those observed in MOPDII, including spindle misorientation and decreased levels of PCNT at the mitotic spindle poles. However, in contrast to what is seen with MOPDII cells, ZIKV infection also resulted in a decrease in PLK1 levels and increases in γ-tubulin and NuMA.

Viral Infection of Neural Progenitor Cells Produces Spindle Misorientation

We next infected a human neural progenitor cell line, H9, with ZIKV (PRVABC59, MOI 5). Analysis of confocal imaging of H9 cells at 24 hpi detected an increase in the spindle angle from 3° in uninfected cells to 15° in infected cells (Figures 2A and 2B). In addition, these studies demonstrated a 33% loss in the intensity of PCNT at the spindle poles of infected H9 cells when compared with uninfected control cells (Figures 2A and 2C). Neonatal infection with CMV is associated with microcephaly (Cheeran et al., 2009). Therefore we next challenged H9 cells with CMV (TB40E-GFP, MOI 3). Similar to what we observed with ZIKV infection, CMV-infected H9 cells displayed altered mitotic spindle orientation when compared with uninfected cells (3° versus 18°, Figures 2D and 2E). PCNT intensity at the spindle poles in CMV-infected H9 cells was also decreased to 48% of that recorded in uninfected control cells (Figures 2D and 2F).

A Diverse Set of Viruses Alters the Mitotic Spindle Angle

We next investigated if events similar to those noted above occur with viruses not associated with microcephaly. A549 cells were infected with either DENV (New Guinea C, 1944, MOI 5), a positive-sense single-stranded RNA flavivirus closely related to ZIKV, or IAV (A/WSN/33(H1N1), MOI 0.5), a negative-sense single-stranded RNA orthomyxovirus. Similar to ZIKV infection, DENV-infected cells had altered mitotic spindle angles (mock 6° versus infected 19°) and a 34% decrease in PCNT intensity at the spindle poles when compared with control cells (Figures 3A–3C). IAV infection also resulted in an increase in the spindle angle with infection (mock 4° versus infected 28°), and a 68% decrease of PCNT at the spindle poles in infected versus uninfected cells (Figures 3D–3F). In addition, HepG2 hepatocellular carcinoma cells, infected with HBV (subtype-ayw MOI 0.4), a circular double-stranded DNA hepadnavirus, were also found to undergo alterations in spindle angles (mock 3° versus infected 18°), together with a 42% loss of PCNT signal at the spindle poles with infection relative to controls (Figures 3G–3I). These results revealed that a wide range of viruses, not restricted to flaviviruses, alters the mitotic spindle pole angle and decreases PCNT intensity at the spindle poles.

IFN-α Alters the Mitotic Spindle Angle

Owing to the fact that a diverse set of viruses all induced spindle misorientation, we hypothesized that the host cells' anti-viral IFN response might contribute to these observations. To test this possibility, we first transfected A549 cells with either a non-targeting small interfering RNA (siRNA) (NT) or an siRNA that targets the mRNA of the IFN-α receptor (IFNAR). The 21- merDharmacon siRNAs used in these studies do not trigger an IFN response (Hornung et al., 2004; Kim et al., 2004). We next treated the NT and IFNAR siRNA-transfected A549 cells with IFN-α, infected with ZIKV, or both. After 24 h, we imaged the cells and measured the spindle angle in mitotic cells. These studies showed that exposure to IFN resulted in an increase in the

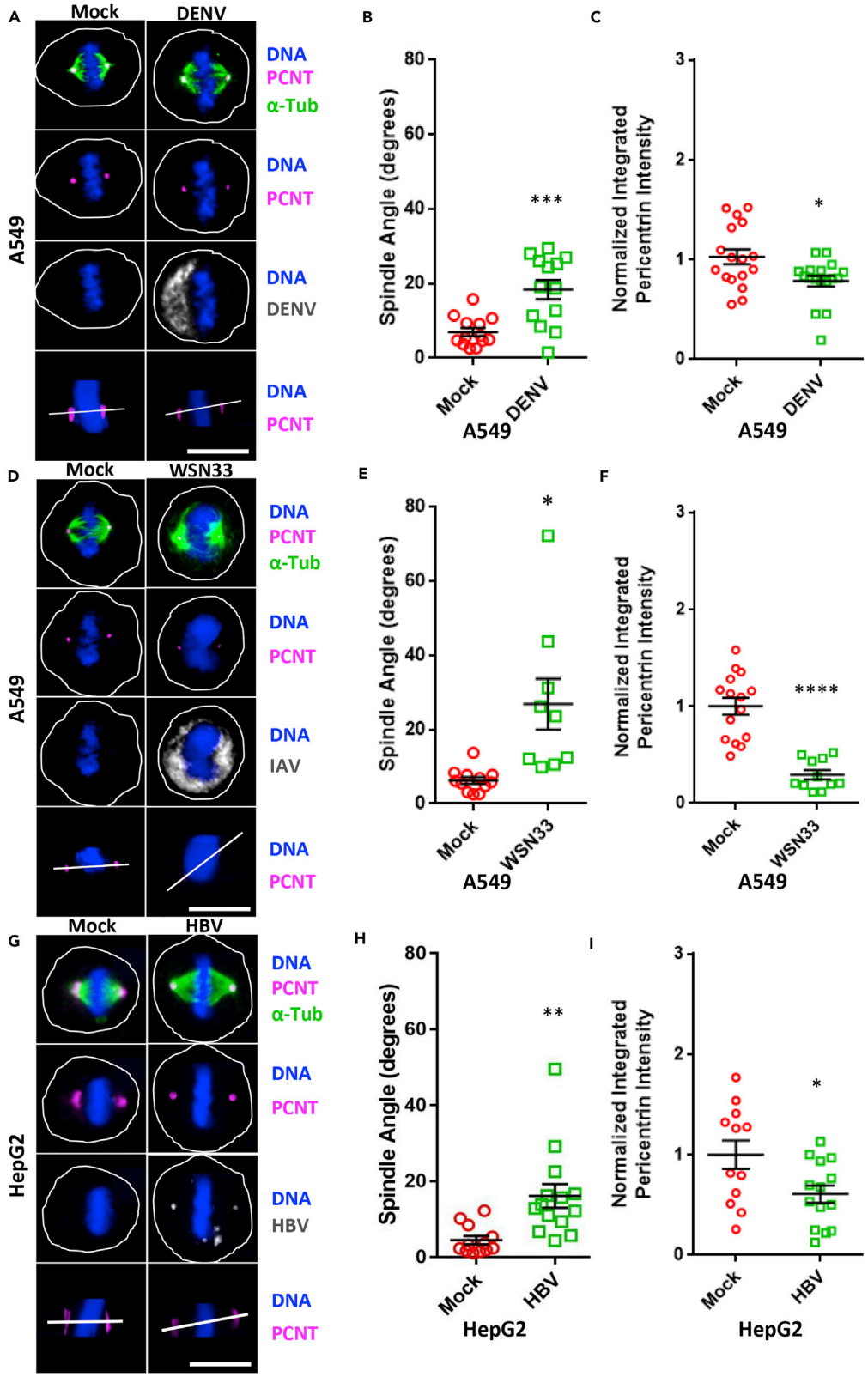
A
Mock
DENV
A549
DNA
PCNT
α-Tub
DNA
PCNT
DNA
DENV
DNA
PCNT
B
Spindle Angle (degrees)
80
60
40
20
0
***
Mock
DENV
A549
C
Normalized Integrated Pericentrin Intensity
3
2
1
0
*
Mock
DENV
A549
D
Mock
WSN33
A549
DNA
PCNT
α-Tub
DNA
PCNT
DNA
IAV
DNA
PCNT
E
Spindle Angle (degrees)
80
60
40
20
0
*
Mock
WSN33
A549
F
Normalized Integrated Pericentrin Intensity
3
2
1
0
****
Mock
WSN33
A549
G
Mock
HBV
HepG2
DNA
PCNT
α-Tub
DNA
PCNT
DNA
HBV
DNA
PCNT
H
Spindle Angle (degrees)
80
60
40
20
0
**
Mock
HBV
HepG2
I
Normalized Integrated Pericentrin Intensity
3
2
1
0
*
Mock
HBV
HepG2

Figure 3. DENV, IAV, and HBV Infections All Produce Spindle Misorientation and Decrease PCNT and PLK1 at the Spindle Poles

(A) Confocal images of A549 cells in metaphase (xz plane), which have been either mock infected (mock) or infected with DENV (New Guinea C MOI 5) for 24 h and immunostained for PCNT (pink), α-Tub (green), or DENV (gray) and stained for DNA (blue). The bottom row of images shows an xz plane with a white line connecting the two spindle poles to approximate the spindle pole angle. Scale bars for all images, 10 μm.

(B) Spindle pole angle quantification for DENV infections of A549 cells for mock infected (red, 13 cells quantitated) and 24 hpi (green, 13 cells).

(C) Quantification of normalized PCNT intensity at the spindle poles for DENV infections of A549 cells analyzed in (B), for mock infected (red) and 24 hpi (green).

(D) Confocal images of A549 cells in metaphase (xz plane), which have been either mock infected (mock) or infected with IAV (A/WSN33/H1N1, MOI 0.5–0.8) for 15 hpi and immunostained for PCNT (pink), α-Tub (green), or DENV (gray) and stained for DNA (blue). The bottom row of images shows an xz plane with a white line connecting the two spindle poles to approximate the spindle pole angle. Scale bars for all images, 10 μm.

(E) Spindle pole angle quantification for IAV infections of A549 cells for mock infected (red, 12 cells quantitated) and 15 hpi (green, 12 cells).

(F) Quantification of normalized PCNT intensity at the spindle poles for IAV infections of A549 cells analyzed in (B), for mock infected (red) and 15 hpi (green).

(G) Confocal images of HepG2-NTCP cells in metaphase (xz plane), which have been either mock infected (mock) or infected with HBV (subtype-ayw MOI 0.4–0.7) for 96 hpi and immunostained for PCNT (pink), α-Tub (green), or DENV (gray) and stained for DNA (blue). The bottom row of images shows an xz plane with a white line connecting the two spindle poles to approximate the spindle pole angle. Scale bars for all images, 10 μm.

(H) Spindle pole angle quantification for HBV infections of HepG2 cells for mock infected (red, 12 cells quantitated) and 96 hpi (green, 12 cells).

(I) Quantification of normalized PCNT intensity at the spindle poles for HBV infections of HepG2 cells analyzed in (B), for mock infected (red) and 96 hpi (green). Statistical significance (p value) of the angle changed or integrated intensity between mock and a condition in all quantified data is represented using asterisks above the data; ****$p < 0.0001$, ***$p < 0.001$, **$p < 0.01$, and *$p < 0.5$. All data represent the mean ± SEM from three independent experiments.

spindle angle, from an average angle of 8.4° in the untreated cells to 19.7° in the ZIKV-infected cells, 19.3° in the IFN-treated cells, and 19.2° in the combined IFN-treated and ZIKV-infected cells, and that this effect of IFN was not seen in the IFNAR-depleted cells (Figures 4A and 4B). Of note, IFN-α treatment or the combined treatment of IFN-α and ZIKV infection also produced decreases in the spindle pole intensities of PCNT, and these effects were also dependent on the expression of IFNAR (Figure 4C).

DISCUSSION

The presence of microcephaly in both MOPDII primary dwarfism and congenital ZIKV syndrome led us to hypothesize that similar events may occur in MOPDII cells and cells infected with ZIKV. Indeed, our studies revealed that ZIKV infection resulted in spindle misorientation, in keeping with what we have found to occur in either MOPDII or Pcnt$^{-/-}$ cells undergoing division, and consistent with previous published work on ZIKV (Onorati et al., 2016; Souza et al., 2016; Wolf et al., 2017). We then extended these observations by showing that similar to what we have reported with mitotic MOPDII and Pcnt$^{-/-}$ cells, ZIKV infection resulted in decreased PCNT levels at the spindle poles of mitotic cells and abnormal centrosome maturation. Therefore in both MOPDII cells and ZIKV-infected cells, defects in PCNT recruitment to centrosomes occur in mitotic cells resulting in spindle misorientation. In contrast to what we have observed in MOPDII cells, ZIKV infection decreased the level of PLK1, a kinase that mediates PCNT phosphorylation and centrosome maturation.

Given the critical role of centrosome maturation in mitotic spindle orientation, it is likely that these observed decreases in PCNT and PLK1 result in the aberrant spindle pole angles seen with ZIKV infection (Chen et al., 2014; Doxsey et al., 1994; Kaltschmidt et al., 2000). The growth and maintenance of the neural stem cell pool is critically important for brain development, with proper cell divisions playing a central role in stem cell health (Gomez-Lopez et al., 2014). Because mitotic spindle orientation has been shown to be important for proper cell division and the maintenance of the neural progenitor pool during brain development (Gomez-Lopez et al., 2014), our findings suggest that viral-associated deficiencies in centrosome maturation, similar to those seen with MOPDII, perturb neural stem cell mitoses, thereby contributing to the development of microcephaly in congenital ZIKV syndrome (Buchman et al., 2010).

Loss of symmetric progenitor divisions likely diminishes the neural progenitor cell population, thus reducing the number of cells available for proper brain development. Indeed, this is precisely what we

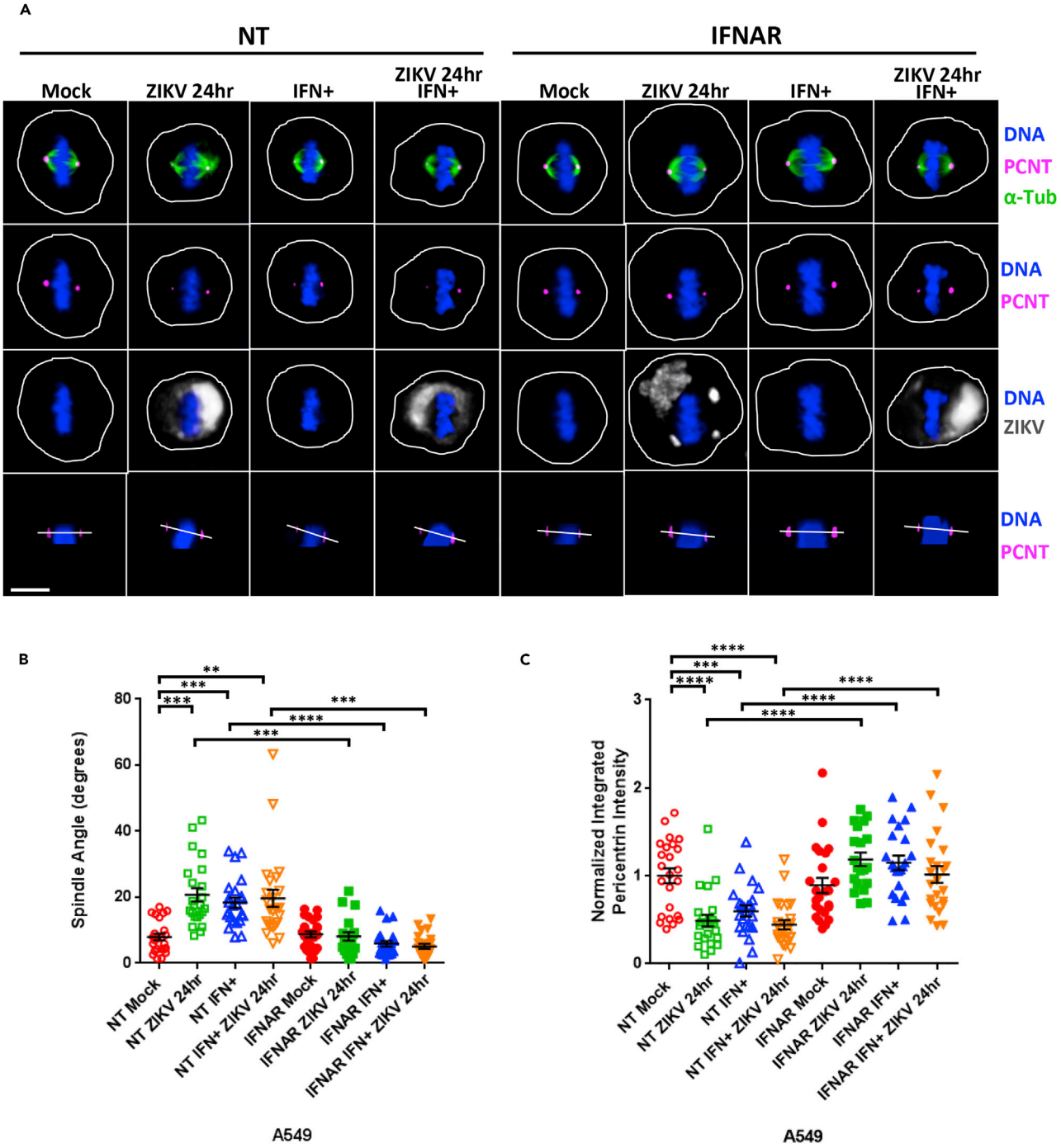

Figure 4. IFN-α Induces Spindle Pole Misorientation and Decreased PCNT at the Spindle Poles

(A) A549 cells were transfected with either a non-targeting negative control siRNA (NT) or an siRNA targeting the IFN-α receptor, IFNAR1 (IFNAR). Forty eight hours post-transfection the cells were incubated without or with IFN-α (+, 100 IU/mL) for 24 h, then either mock infected (mock) or infected with ZIKV (PRVABC59 MOI 5) for 24 h, and immunostained for PCNT (pink), α-Tub (green), or ZIKV (gray) and stained for DNA (blue). Scale bars for all images, 10 μm.

(B) Spindle pole angle quantification for ZIKV infections or IFN-α addition to A549 cells treated with siRNA(NT) in mock infection (red, 16 A549 cells quantitated), 24 hpi (green, 16 cells), IFN-α treatment (blue, 15 cells), and IFN-α + 24 hpi (orange, 16 cells); siRNA(IFNAR) mock infection (solid red, 16 cells), 24 hpi (solid green, 13 cells), IFN-α treatment (solid blue, 16 cells), and IFN-α + 24 hpi (solid orange, 16 cells).

(C) Quantification of normalized PCNT intensity at the spindle poles for A549 cells analyzed in (A and B). Statistical significance (p value) of the angle changed or integrated intensity between mock and a condition in all quantified data is represented using asterisks above the data; ****$p < 0.0001$, ***$p < 0.001$, **$p < 0.01$. All data represent the mean ± SEM from three independent experiments.

have observed in the aberrant developmental phenotypes seen in human primordial dwarfisms and mouse mutations with microcephaly. Therefore further insights into congenital ZIKV syndrome will likely come from the continued study of genetic disorders with similar clinical phenotypes.

We next examined the specificity of viral-induced spindle misorientation, and found that DENV, a flavivirus closely related to ZIKV, also caused this effect in mitotic cells, confirming previous work (Wolf et al., 2017). We then found that aberrant spindle angles were also seen in mitotic cells infected by a broad range of viruses, including CMV, IAV, and HBV, only one of which, CMV, is associated with microcephaly (Cheeran et al., 2009).

These studies demonstrate that infection by positive- and negative-sense RNA viruses, as well as two distinct DNA viruses, all decreased spindle-pole-associated PCNT levels, resulting in perturbations in the spindle pole angles of dividing cells. Thus decreased levels of PCNT at the spindle poles and spindle misorientation are not restricted to infections by microcephaly-inducing viruses such as CMV and ZIKV, but instead are events that occur with many, if not all, viral infections. Although the generality of this last statement remains to be tested with additional viruses, the data nevertheless point toward a common mechanism underlying these events.

In that regard, we deemed it unlikely that each virus had independently evolved a means to alter the cell's spindle angle and decrease PCNT levels; instead we favored the idea that the host cell's innate immune response plays a role. This led us to test the effects of IFN-α on dividing cells. These experiments showed that exposure to IFN-α induced spindle misorientation and decreased the spindle pole levels of PCNT, arguing that the innate immune system's reaction to infection contributes to the observed phenotypes and therefore may impact stem cell health. To determine whether non-specific viral stressors or cellular responses to IFN are culpable for the observed mitotic defects, we exposed cells to IFN-α or ZIKV to mitotic cells after knockdown of IFNAR. In all conditions assayed, depletion of INFAR prevented the loss of PCNT and changes in spindle angles, thus suggesting that effect of IFN-α is the major contributor of these defects. This is consistent with recent studies in mice showing that whereas $Ifnar^{+/-}$ fetuses are more resistant to ZIKV infection compared with $Ifnar^{-/-}$ littermates, an intact IFN response during ZIKV infection results in detrimental side effects, in particular delayed fetal growth and fetal resorption (Yockey et al., 2018). It remains to be determined if other viral infections will also show the same dependence on IFN signaling as ZIKV, and thus the severity of these phenotypes may vary across viruses even in the setting of comparably induced IFN responses.

The finding that IFN-α induces mitotic spindle misorientation suggests that a systemic effect on cell division may occur during IFN-eliciting infections, or with the clinical use of IFN as therapy. In the setting of an infection an IFN-α gradient is created, suggesting the possibility that cells at the most active sites of infection are subjected to the highest IFN levels and could therefore experience the greatest effect on their mitoses. For example, in the case of ZIKV encephalitis *in utero*, the divisions of neural stem cells in the developing brain would be the most affected, whereas in the setting of HBV hepatitis, the dividing liver stem cells would be predominantly affected. In both instances we envision that IFN-altered mitoses could affect stem cell fate and impede organ growth and regeneration.

Limitations of the Study

This study focused solely on the effect of viral infection or IFN-α treatment on mitotic cells in cell culture. Future studies will need to focus on studying this effect in the developing embryos of pregnant mice to establish a clear link between IFN-α, spindle angle disruption, and microcephaly. Furthermore, it remains unclear if other cytokines can cause spindle angle asymmetry in mitotic cells. Moreover, the mechanism by which IFN-α signaling induces asymmetric cell division is currently unknown, and future experiments will be needed to determine which IFN stimulated gene or genes are responsible for this observation.

METHODS

All methods can be found in the accompanying Transparent Methods supplemental file.

SUPPLEMENTAL INFORMATION

Supplemental Information includes Transparent Methods and one figure and can be found with this article online at https://doi.org/10.1016/j.isci.2019.01.025.

ACKNOWLEDGMENTS

This work was funded by an Investigators in the Pathogenesis of Infectious Disease grant from the Burroughs Wellcome Fund to A.L.B. A.L.B. is grateful to the Bill and Melinda Gates Foundation and to Gilead Sciences Inc. for their support.

AUTHOR CONTRIBUTIONS

W.M.M., J.M.P., H.-F.H., A.V., W.Z., X.E., T.F.K., S.D., and A.L.B. performed experiments and wrote the paper.

DECLARATION OF INTERESTS

The authors declare no competing financial interests.

Received: July 7, 2018
Revised: November 1, 2018
Accepted: January 15, 2019
Published: February 22, 2019

REFERENCES

Buchman, J.J., Tseng, H.C., Zhou, Y., Frank, C.L., Xie, Z., and Tsai, L.H. (2010). Cdk5rap2 interacts with pericentrin to maintain the neural progenitor pool in the developing neocortex. Neuron *66*, 386–402.

Cheeran, M.C., Lokensgard, J.R., and Schleiss, M.R. (2009). Neuropathogenesis of congenital cytomegalovirus infection: disease mechanisms and prospects for intervention. Clin. Microbiol. Rev. *22*, 99–126, Table of Contents.

Chen, C.T., Hehnly, H., Yu, Q., Farkas, D., Zheng, G., Redick, S.D., Hung, H.F., Samtani, R., Jurczyk, A., Akbarian, S., et al. (2014). A unique set of centrosome proteins requires pericentrin for spindle-pole localization and spindle orientation. Curr. Biol. *24*, 2327–2334.

Delaval, B., and Doxsey, S. (2008). Genetics. Dwarfism, where pericentrin gains stature. Science *319*, 732–733.

Delaval, B., and Doxsey, S.J. (2010). Pericentrin in cellular function and disease. J. Cell Biol. *188*, 181–190.

Doxsey, S.J., Stein, P., Evans, L., Calarco, P.D., and Kirschner, M. (1994). Pericentrin, a highly conserved centrosome protein involved in microtubule organization. Cell *76*, 639–650.

Gabriel, E., Ramani, A., Karow, U., Gottardo, M., Natarajan, K., Gooi, L.M., Goranci-Buzhala, G., Krut, O., Peters, F., Nikolic, M., et al. (2017). Recent Zika virus isolates induce premature differentiation of neural progenitors in human brain organoids. Cell Stem Cell *20*, 397–406.e5.

Gomez-Lopez, S., Lerner, R.G., and Petritsch, C. (2014). Asymmetric cell division of stem and progenitor cells during homeostasis and cancer. Cell Mol. Life Sci. *71*, 575–597.

Hall, J.G., Flora, C., Scott, C.I., Jr., Pauli, R.M., and Tanaka, K.I. (2004). Majewski osteodysplastic primordial dwarfism type II (MOPD II): natural history and clinical findings. Am. J. Med. Genet. A *130A*, 55–72.

Haren, L., Stearns, T., and Luders, J. (2009). Plk1-dependent recruitment of gamma-tubulin complexes to mitotic centrosomes involves multiple PCM components. PLoS One *4*, e5976.

Hornung, V., Schlender, J., Guenthner-Biller, M., Rothenfusser, S., Endres, S., Conzelmann, K.K., and Hartmann, G. (2004). Replication-dependent potent IFN-alpha induction in human plasmacytoid dendritic cells by a single-stranded RNA virus. J. Immunol. *173*, 5935–5943.

Hung, H.F., Hehnly, H., and Doxsey, S. (2016). The mother centriole appendage protein cenexin modulates lumen formation through spindle orientation. Curr. Biol. *26*, 1248.

Kaltschmidt, J.A., Davidson, C.M., Brown, N.H., and Brand, A.H. (2000). Rotation and asymmetry of the mitotic spindle direct asymmetric cell division in the developing central nervous system. Nat. Cell Biol. *2*, 7–12.

Kim, D.H., Longo, M., Han, Y., Lundberg, P., Cantin, E., and Rossi, J.J. (2004). Interferon induction by siRNAs and ssRNAs synthesized by phage polymerase. Nat. Biotechnol. *22*, 321–325.

Lee, K., and Rhee, K. (2011). PLK1 phosphorylation of pericentrin initiates centrosome maturation at the onset of mitosis. J. Cell Biol. *195*, 1093–1101.

Mlakar, J., Korva, M., Tul, N., Popovic, M., Poljsak-Prijatelj, M., Mraz, J., Kolenc, M., Resman Rus, K., Vesnaver Vipotnik, T., Fabjan Vodusek, V., et al. (2016). Zika virus associated with microcephaly. N. Engl. J. Med. *374*, 951–958.

Onorati, M., Li, Z., Liu, F., Sousa, A.M.M., Nakagawa, N., Li, M., Dell'Anno, M.T., Gulden, F.O., Pochareddy, S., Tebbenkamp, A.T.N., et al. (2016). Zika virus disrupts phospho-TBK1 localization and mitosis in human neuroepithelial stem cells and radial glia. Cell Rep. *16*, 2576–2592.

Prosser, S.L., and Pelletier, L. (2017). Mitotic spindle assembly in animal cells: a fine balancing act. Nat. Rev. Mol. Cell Biol. *18*, 187–201.

Rauch, A., Thiel, C.T., Schindler, D., Wick, U., Crow, Y.J., Ekici, A.B., van Essen, A.J., Goecke, T.O., Al-Gazali, L., Chrzanowska, K.H., et al. (2008). Mutations in the pericentrin (PCNT) gene cause primordial dwarfism. Science *319*, 816–819.

Souza, B.S., Sampaio, G.L., Pereira, C.S., Campos, G.S., Sardi, S.I., Freitas, L.A., Figueira, C.P., Paredes, B.D., Nonaka, C.K., Azevedo, C.M., et al. (2016). Zika virus infection induces mitosis abnormalities and apoptotic cell death of human neural progenitor cells. Sci. Rep. *6*, 39775.

Vertii, A., Kaufman, P.D., Hehnly, H., and Doxsey, S. (2018). New dimensions of asymmetric division in vertebrates. Cytoskeleton (Hoboken) *75*, 87–102.

Wolf, B., Diop, F., Ferraris, P., Wichit, S., Busso, C., Misse, D., and Gonczy, P. (2017). Zika virus causes supernumerary foci with centriolar proteins and impaired spindle positioning. Open Biol. *7*.

Yockey, L.J., Jurado, K.A., Arora, N., Millet, A., Rakib, T., Milano, K.M., Hastings, A.K., Fikrig, E., Kong, Y., Horvath, T.L., et al. (2018). Type I interferons instigate fetal demise after Zika virus infection. Sci. Immunol. *3*.

ISCI, Volume *12*

Supplemental Information

Viral Infection or IFN-α Alters Mitotic Spindle Orientation by Modulating Pericentrin Levels

William M. McDougall, Jill M. Perreira, Hui-Fang Hung, Anastassiia Vertii, E. Xiaofei, Wendy Zimmerman, Timothy F. Kowalik, Stephen Doxsey, and Abraham L. Brass

A

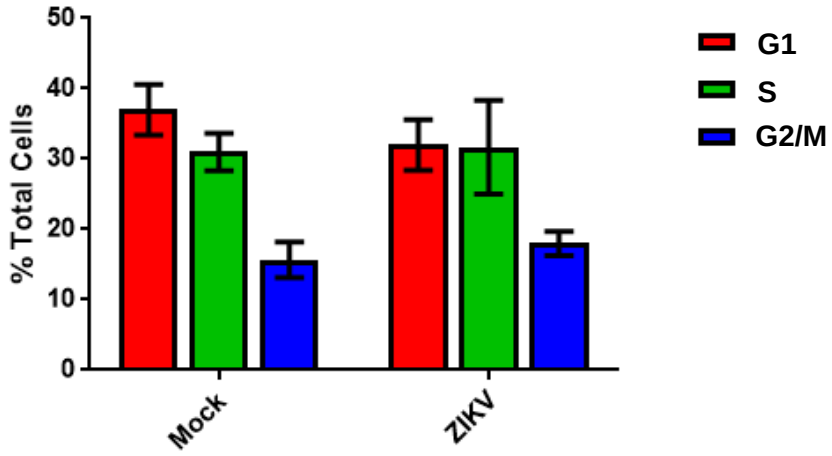

B

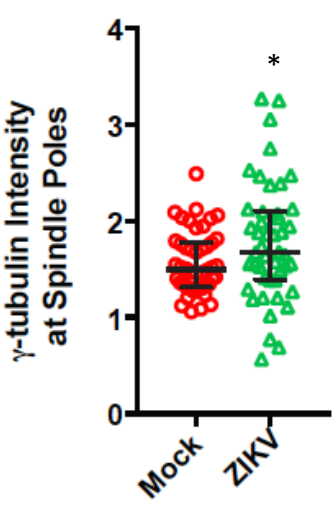

C

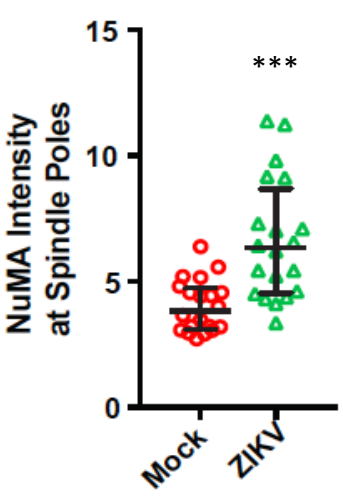

Sup Figure 1

Supplemental Figure 1. Related to Figure 1. ZIKV infection does not alter cell cycle progression, and increases γ-tubulin or NuMA levels at the spindle poles.

(A) Cell-cycle analysis of G0-synchronized A549 cells after ZIKV infection. A549 cells were serum starved for 48 hr, then infected with ZIKV (PRVABC59) at an MOI of 5 for 48 hr. After infection cells were stained with propidium iodine and analyzed for DNA content by flow cytometry. The mean percent cells in G1 (red), S (Green), or G2/M (Blue) phase are shown for either mock infected (mock) or ZIKV-infected samples.

(B) Quantification of γ-Tubulin intensity in the spindle poles of mitotic cells for mock (red, n = 49), or 24 hr (green, n = 48) ZIKV infection.

(C) Quantification of NuMA intensity in the spindle poles of mitotic cells for mock (red, 21), or 24 hr (green, 20) ZIKV infection. Statistical significance (p-value) of the angle changed or integrated intensity between mock and a condition in all quantified data is represented using asterisks above the data, where p-values < 0.001 are "***", and p-values < 0.5 are "*". All data represent the mean +/- SD from three independent experiments.

Transparent Methods

Cell Culture

A549 (ATCC CCL-185), and U2OS (ATCC HTB-96) cells were grown in complete DMEM (Dulbecco's Modified Eagle Media (Sigma, D5671) supplemented with 10% FBS (GIBCO, 10437), 2 mM L-glutamine (GIBCO, 25030), 100 U/mL Pen-Strep (GIBCO, 15140), and Plasmocin (Invivogen, ant-mpt-1). HepG2 (ATCC HB-8065) were transduced with NTCP cDNA using the retroviral transfer vector pQXCIH (Clontech, 631516) to create HepG2-NTCP cells and were grown in complete DMEM. H9 neural progenitors were obtained from Fisher Scientific (N7800100) and grown in KnockOut DMEM/F-12 (GIBCO, 12660) supplemented with 2 mM Glutamax (GIBCO, 35050), 20 ng/mL bFGF (GIBCO, PHG0024), 20 ng/mL EGF (GIBCO, PHG0314) and 2% StemPro Neural Supplement (GIBCO, A10508), and cultured according to manufacturer's instructions.

Viral Culture

ZIKV (Puerto Rico 2015, PRVABC59, ATCC, VR-1843) and DENV (New Guinea C 1944, ATCC VR-1584) were propagated in C6/36 cells grown in RPMI-1640 (Sigma, R0883). After infection for 72 hours supernatants were collected and tittered by infecting A549 cells. HCMV TB40E-GFP virus was generated from electroporation of bacterial artificial chromosome into HEL fibroblasts, and tittered using a standard plaque assay (Paredes and Yu, 2012). HBV (subtype-ayw) was grown in HepAD38 cells cultured in DMEM/F12 (Sigma, D6421) supplemented with 2 mM L-glutamine, 100 U/mL Pen-Strep, and Plasmocin (Ladner et al., 1997). Following weekly collection of media for 4 weeks, viral supernatants are precipitated with 8% PEG8000 (Sigma, 89510) followed by centrifugation at 3500 x g to collect viral particles. HBV titers were determined by infection of HepG2 cells and immunostaining using the HB25B10 hybridoma

supernatants. IAV-A/WSN33/H1N1 was grown by infecting MDCK (ATCC CCL-34) cells grown in complete DMEM. After 72 hrs. of infection supernatants were collected and tittered by infecting A549 cells and immunostaining.

Viral Infections

For ZIKV (PRVABC59), DENV (New Guinea C), and IAV-A/WSN33/ (H1N1) infections, A549 cells were grown to 70% confluence and were infected at an MOI of 5 for ZIKV and DENV, and a MOI of 0.5 for IAV-WSN33 for the indicated time points. H-9 neural progenitor cells were grown to 60% confluence and infected with ZIKV (PRVABC59 MOI 5) for 24 hrs. or were infected with HCMV (TB40E-GFP MOI 3) for 48 hrs. For HBV (serotype-ayw) infections HepG2-NTCP cells were grown to 70% confluence and infected with an MOI of 0.4-0.7 for 24 hr. After 24hr of HBV infection media was replaced with D10G containing 2.5% DMSO (Sigma, D2660) and allowed to incubate for 5 days. After all infections, cells were fixed using 4% Formalin and processed as described below.

Immunostaining and immunofluorescence

Coverslips with the indicated adherent cells were first fixed in 4% formaldehyde (Sigma F8775) in D-PBS (Invitrogen, D8537) for 7 min followed by the addition of ice cold methanol and stored at -20 °C. Cells were then permeabilized in 0.1% Triton X-100 (Fisher, BP151) and 0.1% Tween 20 (Sigma, P7949) in D-PBS for 20 min followed by 3 washes in D-PBS. Blocking was performed for 30 min in 1% BSA (BioPharm, 71-010) in D-PBS containing 0.3 M glycine (Sigma, G7126). Cells were next incubated in primary antibodies (please see antibodies methods section) diluted in 1% BSA in D- PBS for 1 hr, followed by 3 washes with D-PBS. Cells were then incubated in secondary antibodies (see antibodies) diluted 1:1000 in D-PBS containing 1% BSA. Cells were washed 3 times with D-PBS before mounting to slides using Vectashield with DAPI (4', 6'-diamidino-2-phenylindole, Vector Laboratories, H-1200). Samples were then imaged using a Nikon A1 inverted confocal microscope. All microscope settings were kept constant throughout entirety of a given experiment. All other image analyses and all quantifications were done using the FIJI software.

Imaging and analysis for spindle pole angles

Mitotic cells in metaphase were identified by metaphase plate of DAPI staining and PCNT-labeled spindle poles. Z-stacks of mitotic cells from 5 μm-7 μm were acquired using a Nikon A1 inverted confocal microscope (pinhole 0.9 AU) in 0.2 μm steps to capture the entire height of the cell of interest. Spindle angles were calculated by first measuring the linear and vertical distance between PCNT foci followed by calculating the angle between the axis of the spindle and that of the coverslip using the inverse tangent function (arctan(x)), so that 2 PCNT foci focused in the same z-plane have a calculated spindle orientation of 0°.

Imaging and analysis for fluorescence intensities of PCNT, PLK1, NuMA and γ- Tubulin

Imaging was performed as described above and PCNT and PLK1 intensities were quantified by using the 2D sum projection of the z-stack followed by measurement of the integrated

fluorescence density of the PCNT and PLK1 foci, and subtracting the background intensity. Intensities were then normalized to mock conditions.

Images for NuMA and γ-tubulin were acquired with a Zeiss Axiovert 200M, a Perkin Elmer Ultraview spinning disc microscope and Hamamatsu ORCA-ER camera (100x NA1.4 or 40x NA 1.3 Plan-Apochromat Oil objective). Z stacks are shown as 2D maximum projections (MetaMorph, Molecular Devices). Fluorescence range intensity was adjusted identically for each series of panels. Intensity profiles and fluorescence intensity quantification were obtained from sum projections of Z stacks using MetaMorph software. For fluorescence intensity quantification, computer-generated concentric circles of 60 (inner area) or 80 (outer area) pixels in diameter were used to measure centrosome (inner area) and calculate local background (difference between the outer and inner area) fluorescence intensity.

Immunoblotting

Lysates of ZIKV infected A549 or U2OS cells were created by lysing 1x106 cells in Laemmli Sample Buffer (62.5 mM Tris pH 6.8, 10% Glycerol, 2% SDS, 5% β- mercaptoethanol, 0.004% Bromophenol Blue) then separated on a 4-20% Tris-Glycine SDS-PAGE gel. After transfer to PVDF membrane (Thermo, 88518), membranes were blocked with 5% milk then immunoblotted using the antibodies described below.

Cell cycle analysis

0.2 x10^5 A549 cells were plated into 6-well dishes and allowed to attach for 12hrs. Cells were synchronized in G0 by serum starvation after replacing complete media with DMEM supplemented with 2 mM L-glutamine for 48hrs. Following serum starvation, serum free media was replaced with ZIKV containing media or complete DMEM for 48 hrs. After infection, cells were stained with propidium iodine (Abcam, ab139418) and analyzed for DNA content using a MACSQuant flow cytometer and data was analyzed using a univariate model of DNA content in FlowJo™ where 2N counts were assigned G1- phase, 4N/2N were assigned to S-phase, and 4N were assigned G2/M-phase.

siRNA transfections and IFN-α treatment

A549 cells were transfected with siRNAs (non-targeting NT Dharmacon D-001206-14,or IFNAR Dharmacon, L-020209-00) at a final concentration of 50 nM using Oligofectamine (Invitrogen, 1225201) for 48 hr as previously described. After 48 hr, the media was replaced with fresh complete media containing 100 IU/mL IFN-α (Invitrogen, PCH4014); 24 hr later the cells were fixed and processed as described above.

Antibodies

Primary antibodies used in these studies are D1-4G2-4-15 hybridoma (ATCC, HB-112) used to detect ZIKV and DENV, H18-S210 hybridoma (Coriell, WC00029) used to detect IAV-WSN33, H25B10 Hybridoma (ATCC, CRL-8017) used to detect HBV, Pericentrin (Rabbit pAb Abcam, ab4448, 1:300 dilution), α-tubulin (Rat mAb Abcam, ab6161, 1:50 dilution), α-tubulin-FITC conjugated (Mouse mAb Abcam, ab195887 1:100), GFP antibody (mouse mAb, Santa Cruz, sc-

9996 1:500 dilution), PLK1 (Rabbit pAb Novus Biologics, NB100-547 1:1000 dilution), ZIKV (Rabbit pAb Genetex, GTX133314 1:1000 dilution), NuMA (Rabbit pAb Abcam, ab36999), γ-tubulin (Mouse mAb Sigma, GTU-88).

Secondary antibodies for immunofluorescence were all from Thermo Fisher and used at a 1:1000 dilution: AlexaFluor 488 goat anti-mouse IgG (A11001), AlexaFluor 568 goat anti-rabbit IgG (A11011), Alexa Fluor 647 goat anti-rat IgG (A21247). Secondary antibodies for western blot were purchased from Jackson ImmunoResearch and used at a 1:10,000 dilution: goat anti-mouse IgG-HRP (115-035-003), goat anti-rabbit IgG-HRP (111-035-003), goat anti-rat IgG-HRP (112-035-003).

Statistical analysis

All p-values were calculated using a student's t-test with Welche's correction in GraphPad Prism.

References

Ladner, S.K., Otto, M.J., Barker, C.S., Zaifert, K., Wang, G.H., Guo, J.T., Seeger, C., and King, R.W. (1997). Inducible expression of human hepatitis B virus (HBV) in stably transfected hepatoblastoma cells: a novel system for screening potential inhibitors of HBV replication. Antimicrobial agents and chemotherapy *41*, 1715-1720.

Paredes, A.M., and Yu, D. (2012). Human cytomegalovirus: bacterial artificial chromosome (BAC) cloning and genetic manipulation. Current protocols in microbiology *Chapter 14*, Unit14E 14.